

ACCRETION ONTO THE COMPANION OF ETA CARINAE DURING THE SPECTROSCOPIC EVENT. V. THE INFRARED DECLINE

Amit Kashi¹ and Noam Soker¹

ABSTRACT

We propose that the decline in the near-IR flux from the massive binary system η Carinae during the spectroscopic event might be explained by accreted mass that absorbs the radiation from the secondary star, and by that reduces the heating of the dust that is responsible for the near-IR emission. This binary system has an orbital period of 2024 days and eccentricity of $e \simeq 0.9$. The emission in several bands declines for several weeks near every periastron passages, in what is termed the spectroscopic event. In the *accretion model* for the spectroscopic event the secondary star accretes mass from the primary's wind for ~ 10 weeks near every periastron passage. The mass is accreted mainly in the equatorial plane. The disk and its wind block the secondary's radiation from heating dust that does not reside within narrow cones along the symmetry axis. This, we propose, might explain the decline in the near-IR flux occurring at the beginning of each spectroscopic event. We also argue that the increase in the near-IR prior to the event might be accounted for by enhanced hot ($T \sim 1700$ K) dust formation in the collision region of the winds from the two stars. This dust resides within $\sim 60^\circ$ from the equatorial plane, and most of it cannot be heated by the secondary during the accretion phase.

Subject headings: (stars:) binaries: general—stars: mass loss—stars: winds, outflows—stars: individual (η Carinae)

1. INTRODUCTION

The luminous blue variable (LBV) Eta Carinae has been observed and widely studied for almost 170 years, but the existence of its binary companion (Damineli 1996) wasn't

¹Department of Physics, Technion—Israel Institute of Technology, Haifa 32000 Israel; kashia@physics.technion.ac.il; soker@physics.technion.ac.il.

fully accepted until about ten years ago. The two winds blown by the massive stellar binary system are major players in the 5.54 yrs periodicity, as was recognized in the past particularly for the X-ray behavior (Corcoran 2005; Pittard & Corcoran 2002; Akashi et al. 2006). The importance of the secondary star and the colliding winds in explaining the behavior at other wavelengths has emerged only recently (Abraham et al. 2005; Ishibashi et al. 1999; Daminieli et al. 2000; Corcoran et al. 2001; 2004; Hillier et al. 2001; Pittard & Corcoran 2002; Smith et al. 2004; Steiner & Daminieli 2004; Verner et al. 2005; van Genderen et al. 2006; van Genderen & Sterken 2007; Soker 2007; Kashi & Soker 2007a, b; Soker & Behar 2006; Behar et al. 2007).

LBVs are massive stars that are believed to be in a rapid and unstable evolutionary phase in which tens of solar mass of material are ejected into the interstellar medium over a relatively short period of time, possibly in eruptive events (Smith & Owocki 2006; Smith 2007). Such a twenty year long outburst, known as the ‘Great Eruption’, was experienced by η Car in 1843-1863 (Davidson & Humphreys 1997), accompanied by ejection of a mass of $> 12M_{\odot}$ (Smith et al. 2003a; Smith & Owocki 2006; Smith 2007). This ejecta now form a reflecting bipolar nebula—the ‘Homunculus’—which has a dense equatorial gas, and dense clumps above and below the equatorial plane that obscure the central star at many wavelengths. Another outburst, the ‘Lesser Eruption’ occurred between 1887 and 1895, and ejected material mainly in the polar direction, but also in the equatorial direction (Smith 2005; Smith 2005 & Gehrz 1998; Humphreys et al. 1999).

The ejected mass has cooled since the Great Eruption, and formed $\sim 0.1M_{\odot}$ of dust, which obscures the central star, reflects light toward us in other directions, and emits in the IR band (Smith et al. 2003b). The IR luminosity is $L_{IR} \simeq 5 \times 10^6 L_{\odot}$ (Cox et al. 1995; Smith et al. 2003b). According to estimates made by Davidson & Humphreys (1997), this IR emission comprises $\sim 90\%$ of the luminosity emitted by η Car.

The light curve of η Car is characterized by a roughly constant luminosity at all bands, although with fluctuations, for most of the 5.54 yrs orbital period (Whitelock et al. 2004; Falceta-Goncalves et al. 2005; Abraham et al. 2005; Corcoran 2005; Duncan & White 2003; Nielsen et al. 2007). Large variations, typically with slow increase and then rapid decrease that follows by a low state that typically lasts tens of weeks, occur every 2024 days in what is termed the spectroscopic event, after the disappearance of highly ionized lines (Daminieli 1996; Daminieli et al. 2000). The event is thought to occur near periastron passage, where the distance between the two stars is $r = 1.66$ AU (for the binary parameters used by us). In the last periastron passage in 2003.5, for example, the sharp X-ray drop occurred in JD2452819.6 (Corcoran 2005).

In this paper we address the behavior of the near-IR light-curve before and during the

spectroscopic event, attributing the sharp decline in the near-IR to an accretion event. This is the 5th paper in a series of papers aiming at understanding some of the processes during the spectroscopic event by a ~ 10 weeks long accretion event onto the secondary star. The accretion event was proposed to explain the X-ray behavior (Soker 2005; Akashi et al. 2006; Soker & Behar 2006), and was applied to the visible band as well (Soker & Behar 2006; Kashi & Soker 2007b; Soker 2007).

2. THE INFRARED BEHAVIOR NEAR PERIASTRON PASSAGE

2.1. The light curve in the near-IR

In this section we will describe several possible explanations for the near-IR behavior, which we however, find to be problematic. We start by describing the behavior of the near-IR in the *JHKL* bands, from Whitelock et al. (2004; Whitelock, P. 2007 private communication) who presented a detailed near-IR survey of the *JHKL* bands, which was taken for a period of almost 40 years. The flux of the last cycle (the 2003.5 event) can be seen in Fig. 1. The main characteristics of the last cycle are as follows:

1. **Typical flux values.** The longer the wavelength the larger are the average quiescent flux (the flux during most of the time when the system is away from periastron) and the variations in the flux. The average quiescent flux in *J* is ~ 160 Jy, while that in *L* is ~ 1440 Jy.
2. **Rapid increase.** Approximately ~ 150 days before the event a rapid increase in the flux in all wavelengths begins. In *J* and *L* the fluxes reach peak values which are $\Delta F_J \simeq 40$ Jy and $\Delta F_L \simeq 170$ Jy above the average quiescent flux.
3. **The event.** During the event the hard X-ray emission drops to $\sim 1\%$ of the flux before minimum and stays close to that level for about 70 days (Corcoran 2005; Hamaguchi et al. 2007). The IR event is preceded by a brightening at all near-IR wavelengths, as is the case for the X-ray light curve. However, in marked contrast to the X-ray light curve the near-IR fluxes decrease during the event by only $\sim 15 - 24\%$. Only in the *L* band the light curve is flat-bottom, and only for ~ 20 days. While the oscillations in the X-ray flux make it difficult to pinpoint the time of ingress, it is clearly earlier than it is at IR wavelengths. Within the near-IR light curves ingress starts earliest at *L* and latest at *J* where it is more or less coincident with the well-determined start of X-ray flat minimum; the delay between *L* and *J* is ~ 7 days. The *K* minimum occurs at X-ray phase 0.011 (~ 22 days after the beginning of the flat X-ray minimum). We

will attribute the delay of the J ingress to the formation of extra hot dust close to the secondary star near periastron passages.

4. **Typical variation amplitude.** Both the relative and absolute decline (the V-shaped part of the light curves) during the event are larger for longer wavelengths, being $\Delta F_J \simeq -35$ Jy, and $\Delta F_L \simeq -400$ Jy from peak to minimum. In the L band the minimum flux in the event is below the average quiescent flux.
5. **Recover.** After the sharp decline, the L band recovers to more or less its average quiescent flux, while in the JHK bands the fluxes recover to values above the average quiescent flux, and only after the event (lasting ~ 10 weeks) they decline slowly to the quiescent level.

2.2. Problems with a free-free emission model

Whitelock et al. (2004) argued that the main contribution to the $JHKL$ flux variations are due to free-free emission. We now show that this explanation is problematic since free-free emission cannot provide enough flux to explain the observations. We assume that the recombination rate $\dot{R} = \alpha_B \int n_e n_i dV$, is in equilibrium with the ionizing photon emitted by the secondary star per unit time $\dot{\Phi}_2 = 2.5 - 4.4 \times 10^{49} \text{s}^{-1}$ (see Kashi & Soker 2007a). Here n_e , n_i , and dV are the electron number density, ions number density and a unit volume, respectively. Using this assumption to substitute for $\int n_e n_i dV$ in the expression for the free-free emission in the near-IR (Rybicki & Lightmann 2004) we find the contribution of free-free emission to the observed flux

$$F = 22 \left(\frac{\dot{\Phi}_2}{4.4 \times 10^{49} \text{s}^{-1}} \right) \exp \left[-1.44 \left(\frac{\lambda}{1 \mu\text{m}} \right)^{-1} \right] \text{Jy}. \quad (1)$$

We took $T = 10^4$ K in equation (1) (for other values of T the emission will be about the same or lower), and $D_\eta = 2.3$ kpc as the distance to η Car (Davidson & Humphreys 1997). We also used $g_{ff} \simeq 1.2$ as the Gaunt factor in the near-IR. The expected flux in the near-IR as given by equation (1) is plotted in Fig. 2.

Fig. 2 shows that the fluxes the free-free emission can supply, e.g., $F_J = 5.8$ Jy and $F_L = 12$ Jy, are much smaller than the typical variations in fluxes as can be seen in Fig. 1. The ionization by the primary star was not taken into account. Adding it to the ionizing photon rate of the secondary star would increase the flux by 20% at most. Moreover, these results were obtained using 100% production efficiency, and the maximum accepted value for

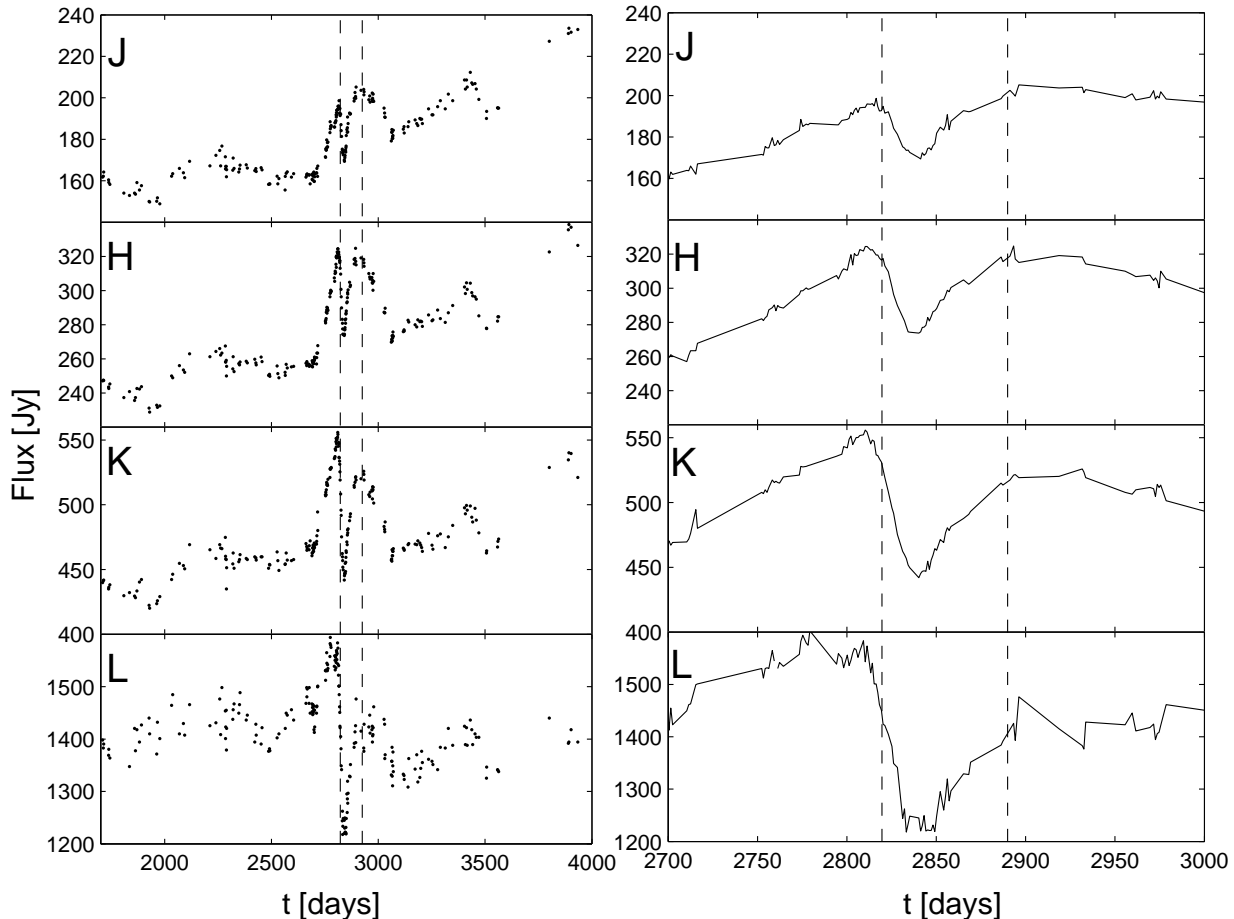


Fig. 1.— Left: The *JHKL* fluxes for the last cycle taken from Whitelock et al. (2004; Whitelock, P. 2007 private communication), from top to bottom, respectively. Right: Zooming on the 2003.5 event. The left vertical lines in both sides of the figure mark the X-ray decline (Corcoran 2005). The right vertical lines mark the end of the assumed 10 week-long accretion process (Soker 2005; Akashi et al. 2006) as discussed in section 6.

the recombination rate \dot{R} , so we expect the free-free contribution to the near-IR flux to be even smaller. We conclude that the free-free emission cannot explain the near-IR behavior.

We emphasize that our calculated changes in the flux near periastron are attributed to ionization by the secondary. The changes, according to the free-free model we are examining here, are due to the dense gas in the colliding wind region. This gas must be ionized. The primary is much cooler than the secondary, and despite being five times as luminous as the secondary has a much lower ionizing flux. Fig. 2 shows that the ionizing radiation cannot explain the changes. More problematic to the free-free emission model is the fact that both

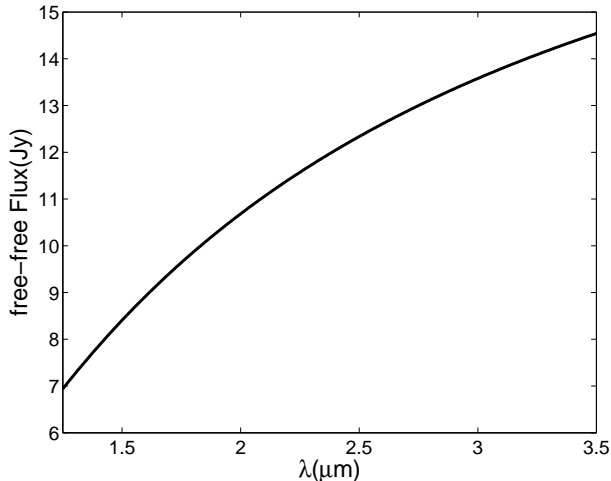


Fig. 2.— The free-free flux in the near-IR as given by equation 1.

the quiescent flux and the variations are larger in the L band than in the K band. The free-free emission from the primary wind is expected to behave in the opposite manner as in the case of the wind of P Cygni (Lamers et al. 1996). Therefore, although the primary wind does contribute to the near-IR emission via free-free emission, it cannot be the main near-IR source. Indeed, in P Cygni the near-IR flux is two orders of magnitude below that in Eta Car (Lamers et al. 1996).

2.3. Problems with a free-free absorption

We now show that the free-free absorption cannot lead to sharp decline in the near-IR during the event. The absorption can be explained in principle by the dense conically-shaped post-shock primary wind. The decline during the event in J is $\sim 15\%$ and in L it is $\sim 24\%$ (section 2.1). The free-free optical depth in the L band is ~ 8.4 times larger than that in J . Therefore, extinction by $\sim 15\%$ in the J band implies almost completely extinction of the L band. The similar decline in J and L can be solved in principle if the dense material covers all (or most) of the hot dust emitting in the J band, and absorbs $\sim 15\%$ of it. The same dense gas covers and completely absorbs only $\sim 24\%$ of the radiation from the warm dust responsible for the L band. This requires a special geometry.

Another problem with such an absorbing model is that there is no good candidate for an absorber:

1. The dense primary wind close to the primary covers a too small angle, considering that

the orbital plane is inclined by $\sim 45^\circ$ to the line of sight, and the IR emitting region is expected to be large.

2. The dense post-shock primary wind material (the conical shell) cannot absorb enough of the J -band emission. For details see Appendix A.
3. The ejection of a dense shell as a general explanation for the spectroscopic event of η Car (Zanella et al. 1984) is ruled out by the X-ray behavior (Akashi et al. 2006).

We therefore regard any model for the sharp decline in the near-IR that is based on a dense gas that obscures the IR emitting regions as unlikely.

2.4. Problems with decreasing dust formation rate

Another model that can account in principle for the sharp decline in the near-IR is based on a fast decline in dust formation during the event. Although we do argue for near-IR emission from dust, an explanation based on a decrease in the dust formation rate for the near-IR decline cannot work for η Car. The decline in the dust formation rate occurs because of a decline in the supply of matter from the binary system and/or an enhanced emission that prevents the matter from cooling and forming dust. In either cases we would expect that the dust residing closer to the binary system will be influenced first, namely, the hotter dust. The hotter dust contributes to the shorter IR wavelengths, and would imply that the J -band decline occurs before the L -band decline. This is contrary to observation (Whitelock et al. 2004; see Fig. 1 here).

3. FITTING THE LIGHTCURVE

Cox et al. (1995) explained the IR light curve of η Car by a modified blackbody emission from dust at two temperatures: A cold dust component at 210 K, and a warm dust component at 430 K. We are interested in the hot dust, and for that we will not modify the fitting of the cold dust as was done by Smith et al. (2003b; see below), but rather only add a third hot component, to better fit the $JHKL$ bands. We will use the same two dust components and the modified blackbody function as in Cox et al. (1995)

$$\tilde{B}(T) = QB(T) = \left(\frac{\lambda}{\lambda_0}\right)^{-m} B(T), \quad (2)$$

where $B(T)$ is the usual Planck function, and $m = 1$ for amorphous Carbon grains (Hildenbrand 1983).

In choosing the temperature of the hot dust component we note that Smith et al. (2007) used hot dust at $T = 1660 - 1750$ K to explain the emission from SN2006jc. They claimed that although the shape of the red continuum excess can be approximately fit by a $T \sim 2000$ K Planck function, optically thin emitting dust grains will have wavelength-dependent emissivity and as long as the grains are not larger than about $a = 1 \mu\text{m}$, the dust will typically have emissivity proportional to λ^β with $-1 \leq \beta \leq -2$. This model is similar to the modified blackbody function of Cox et al. (1995). The work of Smith et al. (2007) suggests that dust can also reach temperatures of $T \sim 1700$ K in an environment similar to that in the colliding winds of η Car. Following the above discussion, we will take the dust in η Car to be composed of three components: Hot dust at $T = 1700$ K, warm dust at $T = 430$ K, and cold dust at $T = 210$ K. We emphasize that we expect the dust in η Car to have a continuous range of temperatures, and therefore the three dust components used by us should be regarded as a representative description of the real situation (a ‘toy model’). Smith et al. (2003b), for example, fit the cold dust with two temperatures of 200 K and 140 K. We are not interested in the cold dust in this work, and present the cold dust with only one temperature. For that we chose a temperature of 210 K. Our fit cannot be used for a quantitative study of the cold gas. In addition, different points in the lightcurve are taken from different sources (as summarized in Cox et al. 1995). For these reasons our treatment of the cold dust is not accurate, and the work of Smith et al. (2003b) that is superior to our fit should be consulted when studying the cold dust. This approximate description is sufficient to teach us about the basic physical processes relevant to the near-IR emission. Only the two hotter components, the hot and the warm, are relevant to the *JHKL* wavebands.

We take the average quiescent flux of *JHKL* discussed in section 2, add it to the data collected by Cox et al. (1995), and create a 3-Temperature modified blackbody fit to the entire IR range

$$F(\lambda) = b_{210}\tilde{B}(210 \text{ K}) + b_{430}\tilde{B}(430 \text{ K}) + b_{1700}\tilde{B}(1700 \text{ K}). \quad (3)$$

The coefficients b_i were obtained by the method of least squares adjustment. The results are presented in Fig. 3.

To better understand the behavior of the *JHKL* emission during the cycle, and in particular near the event we fit the flux from Whitelock (2004) only with the two higher temperature components, and as a function of time

$$F(\lambda, t) = b_{430}(t)\tilde{B}(430 \text{ K}) + b_{1700}(t)\tilde{B}(1700 \text{ K}). \quad (4)$$

We then converted these coefficients to the luminosity of each dust component by integrating over wavelength the modified blackbody flux, and multiplying by $4\pi D_\eta^2$. The luminosity of

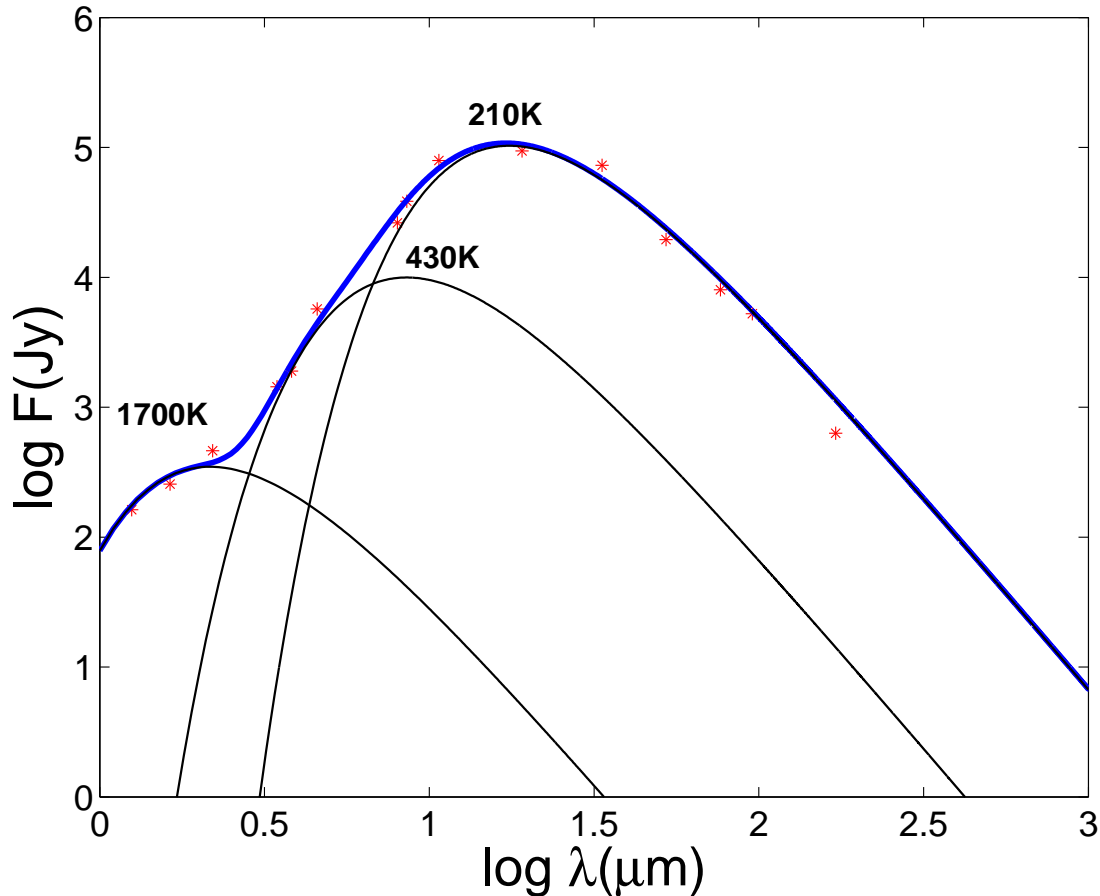


Fig. 3.— Three temperature modified blackbody fit to the IR. The points for the *JHKL* wavebands (4 shortest wavebands) are the average quiescent values from Whitelock et al. (2004), before the beginning of the event. The rest of the points are taken from different sources, summarized in Cox et al. (1995). Each modified blackbody is presented by a thin black line, and the overall adjusted flux is presented by a thick blue line.

the warm and hot dust components as function of time, and in units of their respective quiescent average, is given in Fig. 4.

4. DUST PROPERTIES

Using standard references (e.g., Hildenbrand 1983; Krugel 2003; Whittet 2003) we take the following steps. We assume spherical dust grains with radius $a = 0.25\mu\text{m}$ and density $\rho_d \sim 1.9 \text{ g cm}^{-3}$ (Hildenbrand 1983). The ratio Q/a , where Q is the coefficient of the

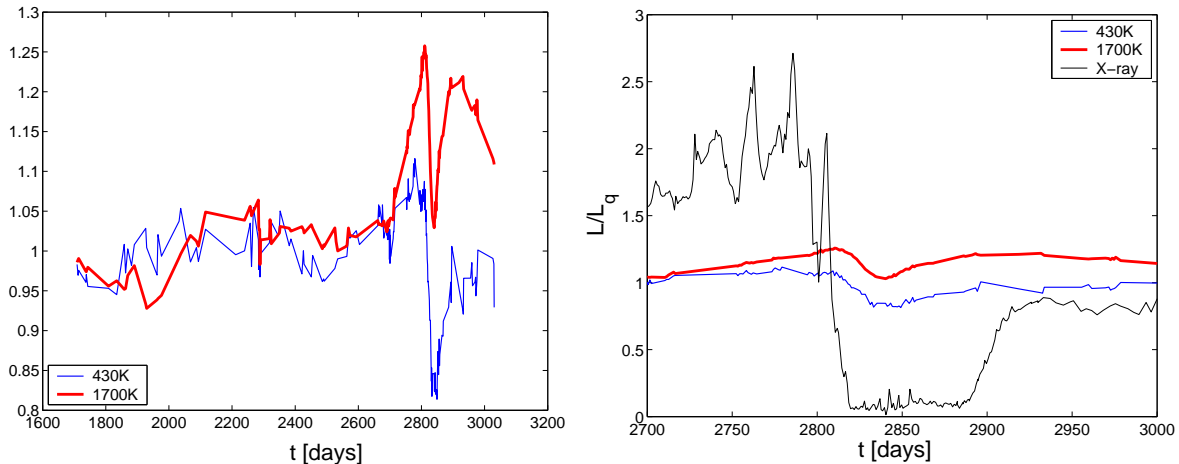


Fig. 4.— The luminosity of the hot (1700 K; upper red line) and warm (430 K; lower blue line) dust components in units of their respective average quiescent value L_q . The left panel show an extended period, while the right panel zoom in on the 2003.5 event, together with the normalized X-Ray flux (from Corcoran 2005). The X-Ray flat minimum begins at $t = 2819.6$.

modified blackbody emission (equation 2), is obtained from figure 8.1 of Krugel (2003), by approximating the wavelengths' range $1\mu m \leq \lambda \leq 100\mu m$

$$\frac{Q}{a} \simeq \frac{7.93}{\lambda}. \quad (5)$$

For our assumed grain radius $a \sim 0.25\mu m$ (Hildenbrand 1983; Andersen 2007) we find $\lambda_0 \simeq 2\mu m$ (see equation 2).

We will now consider a spherical dust grain with a radius a , distance r_d from the star, and at equilibrium with the stellar radiation. The grain is heated mainly by the UV radiation of the star, which has luminosity L_* . At the UV band the absorption factor for dust is $Q \sim 1$. The cross section of the spherical dust grain is taken as $\sigma = \pi a^2$, although it is considered a bit larger in some models. The dust will emit the radiation isotropically as the modified blackbody (equation 2). The thermal equilibrium is expressed as

$$\sigma \frac{L_*}{4\pi r_d^2} = 4\pi a^2 \cdot \pi c \int_0^\infty \tilde{B}(T) \lambda^{-2} d\lambda. \quad (6)$$

where T is the dust temperature. After integrating over the modified blackbody, we get

$$r_d = 26.8 \text{ AU} \left(\frac{L_*}{9 \times 10^5 L_\odot} \right)^{\frac{1}{2}} \left(\frac{T}{1700 \text{ K}} \right)^{-\frac{5}{2}}, \quad (7)$$

where we scaled the stellar luminosity with the assumed secondary’s luminosity. The reason is as follows. We assume that most of the variation in the hot dust luminosity is from hot dust formed in the shocked primary wind as it collides with the secondary wind. The dense gas of the primary wind close to the primary, and in the conical shock region formed by the wind collision absorb most of the primary radiation (Kashi & Soker 2007a). Cold dust which is distributed at larger distances is heated mainly by the primary stellar radiation, and possibly by the secondary radiation that was not absorbed by the hot dust. Hence we take $L_* = L_1 + L_2 = 5 \times 10^6 L_\odot$ (Cox et al. 1995; Davidson & Humphreys 2000) for $T = 430$ K and $T = 210$ K. We take two cases for the hot dust at $T = 1700$ K : $L_* = L_2 = 9 \times 10^5 L_\odot$ (Verner et al. 2005) as a lower limit, and $L_* = L_1 + L_2$ as an upper limit. The lower limit gives $r_d = 26.8$ AU, as seen from equation 7, and the upper limit gives $r_d = 63.1$ AU. Van Genderen et al. (1994) found $r_d = 63$ AU for $T = 1700$ K using regular blackbody function with totally different parameters which were acceptable at the time.

We can also evaluate the total mass of the dust. By taking the luminosity that $N_d(T)$ grains would produce equal to the observed luminosity obtained by integrating the adjusted flux of each component (equation 3) over wavelength

$$L_d(T) = c \int_0^\infty b_i \tilde{B}(T) \lambda^{-2} d\lambda, \quad (8)$$

we can find the number of grains from the equation

$$L_d(T) = N_d(T) 4\pi a^2 \cdot \pi c \int_0^\infty \tilde{B}(T) \lambda^{-2} d\lambda, \quad (9)$$

and then find the mass of the dust from

$$M_d(T) = N_d(T) \frac{4\pi}{3} a^3 \rho_d. \quad (10)$$

Taking $\rho_d \sim 1.9 \text{ g cm}^{-3}$ (Hildenbrand 1983) for the grain density, and the following observed quiescent luminosity for each dust temperature $L_d(1700 \text{ K}) = 1.1 \cdot 10^5 L_\odot$, $L_d(430 \text{ K}) = 7.7 \cdot 10^5 L_\odot$, and $L_d(210 \text{ K}) = 3.9 \cdot 10^6 L_\odot$, we find the approximate dust mass (only dust, not the inferred total gas mass) $M_d(1700 \text{ K}) \simeq 7.6 \times 10^{-9} M_\odot$, $M_d(430 \text{ K}) \simeq 1.4 \times 10^{-5} M_\odot$, and $M_d(210 \text{ K}) \simeq 8.4 \times 10^{-5} M_\odot$.

In an attempt to estimate the mass of dust that resides at a distance $r_d(T)$ from the binary system we assume that gas flows from the binary system at the terminal velocity of the primary wind $v_1 \simeq 500 \text{ km s}^{-1}$. The time it would take for the gas to arrive at distance r_d from the star is $t_{\text{flow}}(T) = r_d(T)/v_1$. For the primary mass loss rate we take $\dot{M}_1 = 3 \times 10^{-4} M_\odot$, and the conical shock to cover $\sim 1/4$ of the space around the star (see

Kashi & Soker 2007a). Assuming the gas to dust ratio is ~ 100 , the estimated dust mass from flow consideration is

$$M_d^{\text{flow}}(T) \simeq \frac{M_{\text{gas}}(T)}{100} \simeq \frac{1}{400} t_{\text{flow}}(T) \dot{M}_1 = 7 \times 10^{-7} \frac{r_d(T)}{100 \text{ AU}} \frac{\dot{M}_1}{3 \times 10^{-4} M_\odot \text{ yr}^{-1}} M_\odot \quad (11)$$

In this formula the flow time $t_{\text{flow}}(T)$ depends on the distance of the dust, which in turn depends on the dust temperature. We summarize our findings in Table 1.

We emphasize that the last two columns of Table 1 are calculated for the (wrong) assumption that the dust is supplied by the present wind. Clearly, as we explain below and is well known (Smith et al. 2003b), the warm and cold dust cannot be supplied by the present wind. Therefore, for example, the flow time to the warm dust of ~ 18.6 years is not the real flow time. It is the flow time had the dust been supplied by the present wind. The hot dust can be supplied by the present wind. Although our "toy model" does not intend to give exact results to the distances and ages of the dust, but only to give a general picture, we bring and discuss Table 1 here because it emphasizes the differences between the hot dust on one hand, and the warm and cold dust components on the other hand.

From Table 1 we learn that the cold dust, which is responsible for most of the observed IR radiation from η Car (Cox et al. 1995), resides at very large distances from the star, compatible with its ejection during the Great Eruption that ended ~ 150 years ago (Smith et al. 2003b; Smith & Gehrz 1998). A small part of this dust was ejected during the Lesser Eruption ~ 115 years ago, which created circumstellar gas at distances of a few hundred to a few thousand AU from the star, mainly in the polar directions, but some in the equatorial plane as well (Smith et al. 2005). Indeed, the present regular flow from the primary cannot supply the mass required to explain the emission by the cold dust, as $M_d^{\text{flow}} \ll M_d$. As stated earlier, our analysis of the cold dust is not accurate, but meant only to present the basic differences between the hot and cold dust, e.g., that the cold dust cannot be supplied by the present mass loss from η Car. A proper analysis of the cold dust, that includes also colder dust at 140 K, yields even larger dust mass of $\sim 0.1 M_\odot$ (total gas and dust mass of $\sim 10 M_\odot$) in the cold phase (Smith et al. 2003b). The required cold and very cold dust mass of $\sim 0.1 M_\odot$ (a gas mass of $\sim 10 M_\odot$) could be easily supplied by the mass lost during the great eruption (Smith et al. 2003b; Smith 2006; Smith & Ferland 2007). The total luminosity of all three components $L_{\text{tot}} = 4.75 \times 10^6 L_\odot$ is smaller than the assumed luminosity of η Car $L_\eta = 5 \times 10^6 L_\odot$ (Cox et al. 1995). This and our finding that the dust mass can be much smaller than that ejected during the great eruption, implies that some radiation escapes without being absorbed by dust. Probably, mainly along the polar direction (Smith et al. 2003a).

Smith et al. (2003b) have also mapped the dust of η Carinae. They used three different

T (K)	r_d (AU)	$L_d(L_\odot)$	$M_d(M_\odot)$	t_{flow} (yr)	$M_d^{\text{flow}}(M_\odot)$
1700 (lower limit)	26.8	1.1×10^5	7.6×10^{-9}	0.25	$\sim 2 \times 10^{-7}$
1700 (upper limit)	63.1	1.1×10^5	7.6×10^{-9}	0.60	$\sim 5 \times 10^{-7}$
430	1,960	7.7×10^5	5.3×10^{-5}	18.6	$\sim 1.5 \times 10^{-5}$
210	11,756	3.9×10^6	9.6×10^{-3}	111.5	$\sim 8 \times 10^{-5}$

Table 1: The properties of the three dust components. T (K) is the dust temperature assumed in our three dust components model. r_d is the distance of the dust to the star, calculated by assuming that the hot dust is heated either by the secondary star or both stars, while the warm and cold dust components are heated by the primary and some of the secondary radiation (primary and secondary luminosities are given in the text). L_d is the luminosity of each component as calculated from the observed IR flux (equation 8). M_d is the dust mass calculated from the observed luminosity by equations (9) and (10). The last two columns examine whether the present primary wind can supply the dust. Therefore we take the outflow velocity to be $v_1 \simeq 500 \text{ km s}^{-1}$. $t_{\text{flow}} = r_d/v_1$ is the flow time of the gas from the binary system to the dust location r_d . M_d^{flow} is the dust mass residing near r_d crudely calculated from the flow time according to equation (11). The results for the 210 K and 430 K dust show that the present wind cannot supply the dust. Those components resides in the Homoncolus and came from the 19th century eruptions. The 1700 K dust forms close to the binary system and can be supplied by the present wind.

temperatures (140 K, 200 K, 400 K), in their goal to find the total mass and IR luminosity of the Homunculus. For a component at $T = 200$ K they got luminosity $L_{200} = 1.2 \times 10^6 L_{\odot}$ and dust mass $M_{200} = 0.015 M_{\odot}$, for a component at $T = 400$ K they got luminosity $L_{400} = 5.5 \times 10^5 L_{\odot}$ and dust mass $M_{400} = 2 \times 10^{-4} M_{\odot}$. Their total IR luminosity was $L_{IR} = 4.3 \times 10^6 L_{\odot}$ (Smith et al. 2003b). Although using some different parameters our results are quite close to their results.

From Table 1 we also learn that a large part of the warm dust can be formed in the outflow from the primary star, and all the hot dust forms from the primary outflow relatively close to the binary star. In the next section we propose that the hot dust component and part of the warm dust component are formed in the conically shaped post-shock primary wind region. From Table 1 we learn also that if for some reason the outflow from the binary system changes its properties, the change in the emission of the hot dust will lag by ~ 0.25 year = 3 months. This time is longer than the ~ 10 weeks duration of the event. This suggests that the changes in the IR flux during the event is not due to changes in the outflow that forms the dust. The much slower increase in the IR flux starting ~ 150 days before the event can be accounted for by changes in the flow properties, as we explain in the next section. We attribute the rapid changes in the IR fluxes to obscuration of the secondary star by the mass accreted onto it during the event (sections 6.1 and 7).

5. HOT DUST FORMATION

Hot dust is present at all times as is inferred from the J and H bands. It is probably formed in the primary wind, both the shocked and unshocked segments. Here we don't consider the dust formation in the primary wind in quiescence. We only examine the possibility that the increase in the near infrared luminosity close to periastron passage is caused by enhanced dust formation in the shocked primary wind.

The two stellar winds collide and go through two respective shock waves, with a contact discontinuity between the two post-shock wind regions, as drawn schematically in Fig. 5. The post shock primary wind cools fast as it outflows (Kashi & Soker 2007a; Soker 2003; Pittard & Corcoran 2002) and forms a thin shell in a conical type shape, which we refer to as the conical shell. We expect dust to form in this cool high density conical shell. The shocked secondary wind has a very low density and does not cool. No dust will be formed in that region. The density in the conical shell depends on several parameters, e.g., the properties of the secondary winds (Kashi & Soker 2007a). More influential and relevant to the present study is the dependence of density on the primary mass loss rate \dot{M}_1 , on the orbital separation r , on the distance from the primary r_1 , and on the magnetic field in the

primary wind via its influence on the post-shock density (Kashi & Soker 2007a). Typical values of the proton number density in the conical shell are $n_p \simeq 10^9 - 10^{14} \text{ cm}^{-3}$ (Kashi & Soker 2007a). It is interesting to note that Smith et al. (2007) require a density of $n_p \simeq 10^{10} \text{ cm}^{-3}$ to exist in the region where the hot ($\sim 1600 \text{ K}$) dust is formed in SN 2006jc.

We examine the ionization structure of the conical shell as a result of the secondary radiation. Our motivation is to examine whether extra hot dust can be formed in the conical shell as the system approaches periastron, in addition to dust expected to be formed in the primary wind. We neglect the ionizing radiation from the primary because most of it is assumed to ionize the primary wind close to its origin (Kashi & Soker 2007a). We identify three stages of ionization along the orbit: (i) When the orbital separation is large, as is the case for most of the orbital period, the density in the conical shell is low, and reaches only $n \sim 10^9 - 10^{10} \text{ cm}^{-3}$ in the densest parts. Therefore, the hot secondary ionizing radiation manages to keep the conical shell totally ionized. In that stage dust can be formed only at very large distances. Not much hot dust will be formed close to the secondary. The hot dust might be formed in the primary wind and be heated by the primary and secondary radiation which penetrate the conical shell. (ii) In a calculation described in Appendix B below, we find that when the orbital separation decreases to $r \lesssim 14.3 \text{ AU}$ at ~ 170 days before (after) periastron, the density of the gas in the conical shell increases such that the cone starts to be optically thick to the secondary’s UV radiation and parts of the cone begin to be neutral. First at large distances, and then closer and closer to the stagnation point along the line joining the two stars. (iii) As the secondary approaches periastron, $r \lesssim 3.2 \text{ AU}$ at ~ 20 days before (after) periastron the ionization front is within the conical shell in all directions, and the region near the stagnation point becomes neutral, as shown in Figs. 9 and 10 in Appendix B.

According to the parameters used here, stage (ii) starts ~ 170 days before periastron passage. We propose that the favorable conditions for dust formation lead indeed to dust formation close to the secondary star. This hot dust is the explanation for the rapid increase in the near-IR starting ~ 150 days before the 2003.5 event. Considering the many uncertainties, e.g., the value of the magnetic field in the primary wind (see Kashi & Soker 2007a) and the many fluctuations in the near-IR light curve (Whitelock et al. 2004), we consider satisfactory that we find the favorable conditions for hot dust formation, hence the rapid increase in the near-IR flux according to our model, to start ~ 170 days before periastron, while the observations show it to start ~ 150 days before periastron passage in the 2003.5 event. The exact time when the conditions become favorable for dust formation is very sensitive to several of the winds parameters, and therefore we cannot predict the exact time when the favorable conditions for dust formation will start in future events. Indeed, in the

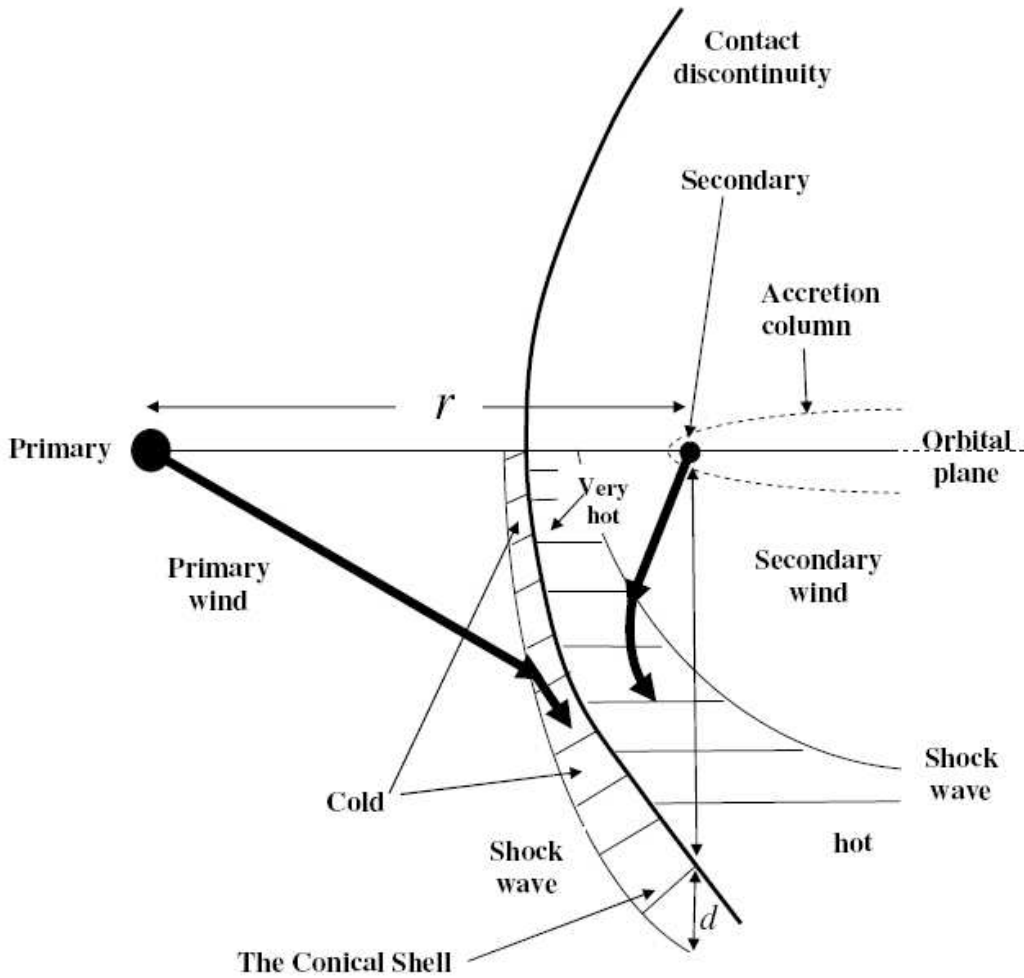


Fig. 5.— Schematic drawing of the collision region of the two stellar winds and the definition of several quantities used in the paper. There is an axial symmetry around the line through the two stars. The two thick lines represent winds’ stream lines. The two shock waves are drawn only in the lower half. The post-shock regions of the two winds are hatched. The shocked primary wind region is referred to as the ‘conical shell’. The dashed line shows the accretion column which exists, according to the proposed model, only for $\sim 70 - 80$ days during the accretion period which corresponds to the X-ray minimum and the spectroscopic event.

1992.5 and 1998 events there is no rapid increase in the near-IR flux before the event, but rather a gradual increase that seems to be part of the secular variation (Whitelock et al. 2004). In the 1981 event there is a rapid rise before periastron, while in the 1987 event the

rapid rise occurs earlier on, starting ~ 300 days before the event and finishing after several tens of days. The secular (gradual) increase in the near-IR flux is observed to occur over the last 4 decades (Whitelock et al. 2004; Whitelock, P. 2007, private communication). In addition to the gradual increase there are slow large flux fluctuations during the orbital period. These fluctuations and the gradual increase will be treated in a separate paper, where the secular increase in the near-IR emission will be attributed to the recovery of *both* the primary (from its high mass loss rate) and the secondary (from its high mass accretion rate) from the ‘Great Eruption’.

The orbital separation ~ 170 days before periastron passage is $r \sim 14.3$ AU. The extra hot dust starts to be formed at a distance of $r_2 \sim 13.4$ AU from the secondary. This is compatible with the distance of the hot dust from the secondary $r_2 \sim 25 - 60$ AU as we found in section 4 (see Table 1).

The hydrogen and helium visible and infrared lines are no problem in explaining near-IR emission from dust, since they are not generated in the same place where the dust resides. The HeI lines are formed in the acceleration zone of the secondary wind (Kashi and Soker 2007b) while the dust emitting the near-IR is formed in the outer regions of the conical shock.

Walsh & Ageorges (2000) discuss dust features in η Car, mainly in the Homunculus. The IR spectrum of η Car is characterized by a peak around $10\mu m$ (Mitchell & Robinson, 1978), indicative of silicate grains (Whittet 2003). Walsh & Ageorges (2000) claim that few percents of the visual and *JHK* radiation is polarized. Polarized radiation is a strong indication for non-spherical grains. Magnetic fields make the grains align more or less with their long axes parallel to each other, causing polarized radiation scattering (Whittet 2003).

The existence of non-spherical silicate grains instead of spherical amorphous-carbon grains, may slightly change $Q(\lambda)$, because the extinction curve for grains from different materials and shape is different (Krugel 2003). Consequently the curve of the modified-blackbody function we used (equations 2 and 5) is changed. These small changes, however, cannot cause a serious change in our results.

6. THE ACCRETION PHASE

In total, the accretion process lasts ~ 10 weeks (Soker 2005; Akashi et al. 2006). We consider two modes of the accretion process; we expect the real accretion process to include both. The discussion below is based on previous papers of the series, in particular Soker (2005b) and Akashi et al. (2006).

6.1. General Considerations

As was explained in previous papers in the series (Soker 2005b; Akashi et al. 2006), there are strong arguments supporting an accretion phase lasting ~ 10 weeks near periastron passage. The disk has time to establish itself because its Keplerian time t_{dd} is much shorter than the length of the accretion phase. For a secondary mass of $M_2 = 30M_\odot$ the Keplerian (dynamical) time at radius r_{dd} in the disk is $t_{dd} \simeq 1.4(r_{dd}/60R_\odot)^{3/2}$ week. We took the accretion disk outer radius to be about three times its inner radius (the secondary radius). The parts of the disk closer to the secondary surface establish themselves in less than a week.

However, the viscous time scale is longer, and the disk does not reach a steady state. The viscosity interaction time to spread material in geometrically thin disks is $t_{vd} \sim 0.1r_{dd}^2/(\alpha_{dd}C_sH)$ (Frank et al. 1985), where $H \simeq (C_s/v_K)r_{dd}$ is the vertical size of the disk, v_K is the Keplerian velocity at r_{dd} , C_s is the sound speed, and $\alpha_{dd} \sim 0.01 - 1$ is the viscosity parameter. This gives that the viscous time scale is

$$t_{vd} \simeq t_{dd} \frac{0.1}{2\pi\alpha_{dd}} \left(\frac{r_{dd}}{H} \right)^2. \quad (12)$$

For $H/r_{dd} \simeq 0.3$ and $\alpha_{dd} \simeq 0.1$, we find the viscous time scale to be somewhat longer than the dynamical (Keplerian) time scale. The viscous time scale might become as long as a few weeks at the outer boundary of the accretion disk (although the time is much shorter close to the secondary surface). In our model, therefore, a disk is formed, but it does not reach a complete equilibrium, and does not settle into a fully thin disk. The disk probably has a wind as part of the evolution toward equilibrium. The disk and its wind block the radiation in most directions, allowing most of the secondary radiation to escape only in narrow cones in the polar directions. This is drawn schematically in Figure 6.

For our purpose any dust residing outside the illuminating cones, i.e., away from the polar directions, is practically close to the equatorial plane (even if geometrically speaking it is not). In particular, this holds for dust that is/was formed in the conical shell. Therefore, most of the excess hot dust that is being formed in the conical shell close to periastron passage will not be heated by the secondary radiation during the accretion phase. The same holds for dust that is being formed in the accretion column during the accretion phase.

The secondary luminosity constitutes $\sim 18\%$ of the total luminosity in our model (see section 4). Because the secondary is closer to the hot dust and a substantial fraction of the primary radiation is blocked from heating the excess hot dust (that was formed in the conical shell) by the primary's own dense wind, the secondary share in heating the excess hot dust is much larger than its $\sim 18\%$ contribution to the bolometric luminosity of the system. Therefore, during the accretion phase the heating of the hot dust can potentially be

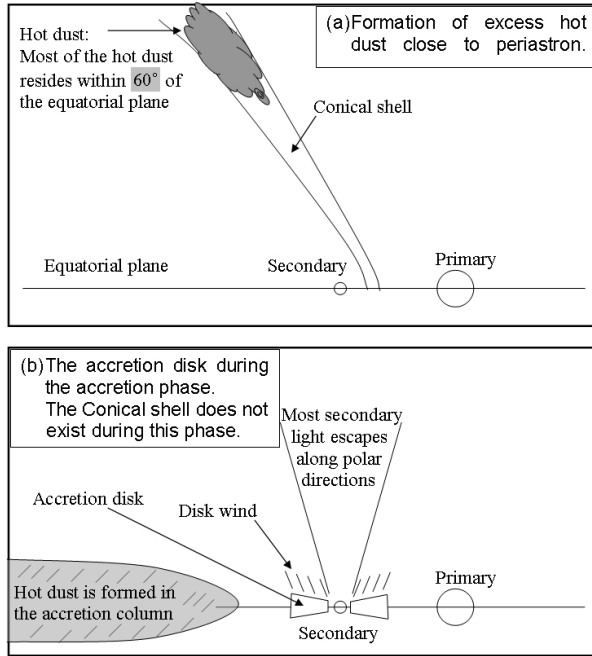


Fig. 6.— Schematic geometry of the hot dust and secondary illumination of the hot dust. Some components are drawn only on one side of the equatorial plane. Upper panel: When the conical shell, formed by the winds’ collision, exists, then the secondary illuminates it in all directions. Lower panel: During the accretion phase. The accretion disk and its wind block the secondary radiation in most directions; radiation escapes in narrow cones along the polar directions. The secondary wind does not exist, or exists only along the polar directions. Hot dust is formed in the accretion column.

reduced more than $\sim 20\%$. As we will discuss below, this is indeed the case.

6.2. The collapse of the conical shell

In the first mode of accretion the conical shell close to the stagnation region collapses first onto the secondary. The optical depth of the conical shell at three orbital phases and as function of direction from the secondary is shown in Fig. 7. For the half space of $\alpha > 90^\circ$ close to periastron passage ($\theta = 0$) we take an average value of $\tau_0 \simeq 0.4$. As this region collapses toward the secondary the optical depth increases as $\tau \gtrsim \tau_0 r_{2s}/r_2$, where $r_{2s} \simeq 0.5$ AU and r_2 are the distances of the shell from the secondary before the collapse starts and after, respectively. The reason the opacity increases faster than $1/r_2$ is that the density increases as $1/r_2^2$ as the conical shell collapses, and with it the opacity. We find that

$\tau \simeq 1$ at $r_2 \simeq 0.3 \text{ AU} \simeq 3R_2$. Because of the non-negligible angular momentum, the mass will be accreted mostly from near the equatorial plane (Akashi et al. 2006).

The stagnation point is at a distance of $\sim 0.5 \text{ AU}$ from the secondary, but regions away from the stagnation point are at larger distances. Taking the last region to collapse to fall from $\sim 1 \text{ AU}$, we find the free fall time to be ~ 12 days, which is about half the duration of the fast decline phase.

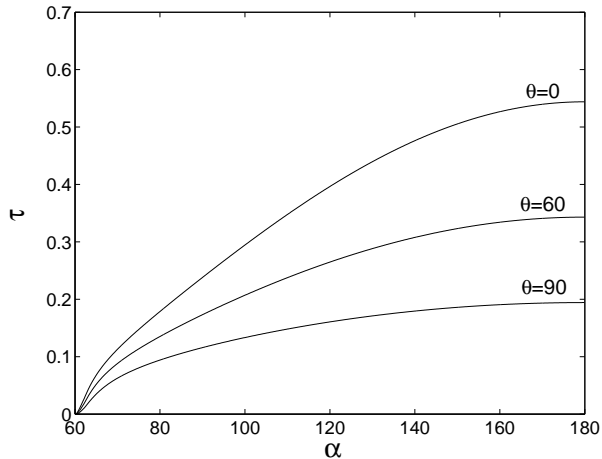


Fig. 7.— The optical depth of the conical shell as a function of direction α and for different orbital angles θ : $\theta = 90^\circ$ and $\theta = 60^\circ$ corresponding to ~ 20 and ~ 9 days before periastron passage, and $\theta = 0$ at periastron passage. $\alpha = 180^\circ$ corresponds to the stagnation point.

6.3. Accretion from the acceleration zone of the primary wind

In the second mode we assume that near periastron passage most of the mass lost by the primary is accreted by the secondary $\dot{M}_{\text{acc}2} \simeq \dot{M}_1$. We note that the accretion rate can be even larger as the primary almost fills its Roche lobe. The primary spin is not synchronized with the orbital motion, and it is probably slower, the true primary's Roche lobe is smaller than calculated for synchronized systems. For an effective temperature of $T_{\text{eff}1} = 20,000 \text{ K}$ and luminosity of $L_1 = 4.5 \times 10^6 L_\odot$ we find $R_1 \simeq 180R_\odot$. Assuming that the primary wind velocity $v_1 = 500 \text{ km s}^{-1}$ is the escape velocity from the primary star, and taking its mass to be $M_1 = 120M_\odot$, we find the same radius $R_1 \simeq 180R_\odot$. The orbital separation between the two stars near periastron is in the range $a_p \simeq 250 - 350R_\odot$ for an eccentricity of $0.93 - 0.9$, respectively. Namely, near periastron $R_1/a_p \simeq 0.5 - 0.75$. The secondary is within the acceleration zone of the primary wind, and the accretion rate can be very high.

Assuming that the mass falls on the secondary at the free fall speed $v_{ff} = (2GM_2/r_2)^{1/2}$, and taking for the secondary mass $M_2 = 30M_\odot$, the density of the accreted matter is

$$\rho_{\text{acc}} = \frac{\dot{M}_{\text{acc}2}}{4\pi r_2^2 v_{ff}} = 3.06 \times 10^{-13} \left(\frac{\dot{M}_{\text{acc}}}{10^{-4}M_\odot \text{ yr}^{-1}} \right) \left(\frac{r_2}{100R_\odot} \right)^{-3/2} \text{ g cm}^{-3}. \quad (13)$$

For a temperature of 10^4 K we find the opacity to be $\kappa \simeq 0.3$. Therefore, the optical depth is

$$\tau \simeq 3 \left(\frac{\dot{M}_{\text{acc}}}{10^{-4}M_\odot \text{ yr}^{-1}} \right) \left(\frac{r_2}{100R_\odot} \right)^{-1/2}. \quad (14)$$

The angular momentum of this material is large, and most of it will be accreted from the equatorial plane. We have no way to estimate the total duration of the high accretion rate phase, and have to assume that it lasts ~ 5 weeks, as the duration of the low IR phase.

Although the conical shell does not exist during the accretion phase, dust continues to form in the accretion column—the dense region formed behind the accreting secondary (see Fig. 5 and previous papers in the series). The high density and high opacity near periastron passage and during the initial accretion phase implies that dust will be formed close to the secondary star. This will be hot dust. Therefore, there are two competing effects at the beginning of the accretion phase. On the one hand obscuration of the secondary radiation in the equatorial plane reduces dust heating. This causes the early decline in the L band. On the other hand dust is formed close to the secondary star. This dust is hot, and contributes mainly to the J band. Initially this effect dominates over the obscuration of radiation, and therefore the flux in J starts to decline later. The delay between the warm and hot dust is seen also in Fig. 4, where the X-ray light curve is also presented. The obscuration becomes the dominant effect when the accretion phase is well developed, when the X-ray drops as well.

The accretion phase continues after the secondary has left the acceleration zone of the primary wind, and lasts for a total of ~ 10 weeks. The accreted gas at the second half of the accretion phase has angular momentum that is not enough to form an accretion disk. However, it is high enough to channel accretion to the equatorial plane; we continue to refer to this equatorial accretion as ‘disk’. The accretion of gas mostly from the vicinity of the equatorial plane during the entire accretion phase results in a collimated polar outflow (wind) that after being shocked emits in the hard X-ray, and accounts for the residual X-ray emission during the event (Akashi et al. 2006 section 4.3.1). The speed of this polar outflow is similar to the secondary wind speed, hence will lead to similar X-ray temperature, as found by Hamaguchi et al. (2007; for that the criticism of Hamaguchi et al. of the accretion model is not valid). We emphasize that we are referring here to a collimated flow blown by

the secondary star. The primary star continues to blow its much more massive wind, which is spherical during the event (Smith et al. 2003a).

This polar outflow will make the optical depth in the polar directions much lower than in the equatorial plane. Hence, a large fraction of the secondary radiation will be emitted along the polar direction during the accretion phase. Because all the excess hot dust (that is formed in the conical shell close to periastron passage) resides within $\lesssim 60^\circ$ from the equatorial plane, and a large fraction of the hot and warm dust that is formed in the unshocked primary wind resides away from the polar directions as well [Smith et al. 2000; cooler dust at $T < 200$ K resides in the polar lobes and larger distances (Smith et al. 2003b; Gomez et al. 2006)], we expect the dust emission to decrease as the disk blocks the secondary radiation; this is the subject of section 7. As the spectroscopic event proceeds, the secondary’s distance from the primary increases, and the accretion rate decreases. The polar opening angle is expected to increase, and more of the secondary radiation will reach regions closer and closer to the equatorial plane, where hot dust resides.

7. DISCUSSION AND SUMMARY: A MODEL FOR THE NEAR-IR LIGHTCURVE

The main goal of this paper is to explain the fast decrease and then increase in the near-IR emission that occurs during the spectroscopic event (Whitelock et al. 2004). For that, we now incorporate all the ingredients discussed in previous sections, and try to explain the near-IR light curve near periastron passage.

In section 2 we argued that free-free emission cannot account for the near-IR behavior. Basically, the free-free emission cannot supply the required luminosity. We also showed that absorption of the near-IR emission cannot account for the decline. In sections 3 and 4 we explored the dust properties, by building a ‘toy model’ where the dust is composed of three-temperature components. We found there that the hot (1700 K) dust can be supplied directly by the present mass loss rate of the primary star. The warm and cold dust, on the other hand, must come mainly from the eruptions of the 19th century and even from earlier times (Smith et al. 2003b; Gomez et al. 2006).

In section 5 we argued that as the two stars approach periastron conditions become favorable for dust formation in the conical shell—the post shock region of the primary wind (see Fig. 5); This is presented in Figs. 9 and 10). We attribute the rapid increase in the near IR flux starting about five months before the 2003.5 event to enhanced dust formation in the conical shell. The conditions are very sensitive to several of the wind parameters of

both stars. Indeed, in some past events there was no rapid rise, while in others the rapid rise occurred at different orbital phases before periastron (see section 5). We therefore cannot predict the exact time for the favorable dust formation conditions, hence the rapid increase in the near-IR flux, to occur in future events. In addition to this sensitivity there is the gradual change in the IR flux observed for almost 40 years now, which we attribute in a future paper to the recovery of *both* the primary and secondary from the Great Eruption of the 19th century.

We turn to describe the decline during the spectroscopic event. In previous papers in the series the absorption of the secondary ionizing radiation was considered (Soker 2007; Kashi & Soker 2007a). Here we are also interested in the near UV and visible bands which are responsible for heating the dust. Our findings in section 6 suggest that the mass accretion rate near periastron passage is such that the secondary radiation capable of heating the dust is almost completely blocked in directions away from the polar directions. Most of the radiation will escape in narrow cones in the polar directions, and some will be converted to longer wavelengths by the optically thick accreted gas. These longer wavelengths are less efficient in heating the dust. We expect some of the hot dust to be formed in the conical shock (section 5), hence to reside within $\sim 60^\circ$ of the equatorial plane. The polar radiation will not heat this dust, and the dust will cool down and the emission in the *JHKL* IR bands will drop. Dust at very large distances will be heated by the primary’s radiation and secondary’s polar radiation, so we expect no decline in the far IR. (e.g., in $\sim 30\mu m$).

Most of the excess hot dust, i.e., the dust that is formed within several months from periastron passage, is heated by the secondary star, that accounts for $\sim 18\%$ of the bolometric luminosity. Therefore, the blockage of the radiation of the secondary will erase almost completely the increase in the near IR radiation prior to the decline. Hot dust that is formed close to the secondary will partially compensate for this decline. More than that, the blocked radiation from the secondary (during the accretion phase) does not heat the dust that is formed in the unshocked primary wind. Therefore, the total decline can bring the radiation to be below its quiescent level.

The high density and high opacity near periastron passage and during the initial accretion phase implies that dust will be formed close to the secondary star. This will be hot dust. Therefore, there are two competing effects at the beginning of the accretion phase. On the one hand obscuration of the radiation of the secondary in the equatorial plane reduces dust heating. This causes the early decline in the *L* band. On the other hand dust is formed close to the secondary star. This dust is hot, and contributes mainly to the *J* band. Initially this effect dominates over the obscuration of radiation, and therefore the flux in *J* starts to decline later. The delay between the warm and hot dust is seen also in Fig. 4, where the

X-ray light curve is also presented. The obscuration becomes the dominant effect when the accretion phase is well developed, at that stage the X-rays sharply drop as well.

We attribute the sharp decline in the near-IR emission near periastron passage (the V-shaped region in the light curve) to the high mass accretion phase occurring at the beginning of the accretion phase (lasting ~ 5 weeks). The Bondi-Hoyle accretion rate of the secondary from the primary wind outside its acceleration zone is $M_{\text{acc}} \simeq 10^{-6} M_{\odot}$ (Akashi et al. 2006), and the optical depth is very low. Therefore, in the second part of the accretion phase (lasting ~ 5 weeks,) when the orbital separation increases, the radiation of the secondary manages to heat more and more dust closer to the equatorial plane, mainly hot dust, and the near-IR emission recovers.

The decrease in the heating radiation from the secondary toward low latitudes starts when matter starts to be accreted on the secondary. This occurs a few weeks before the event. This explains the early small decrease in the L band. At the same time, more dust is formed close to the secondary star. This is a hot dust, that more than compensates which more than compensates for the decrease in the radiation, hence the flux in the J band continues to increase. Eventually, as the accretion phase is developed, there is a rapid decline in all bands.

We suspect that after the high mass accretion rate phase starts, it is mainly the nearby dust that formed in the accretion column that is being heated. This is a relatively hot dust. The secondary does not heat dust at large distances in the equatorial plane, which emits much more in the L band. Therefore, J recovers relatively more than L (in absolute flux L changes more).

At all times the primary continues almost unaffected its role in heating the dust, therefore the decline in the IR is only $\sim 10 - 24\%$.

We are grateful to Patricia Whitlock, Freddy Marang and Francois van Wyk for sending us their data plotted in Fig. 1. We thank Nathan Smith for very helpful comments. This research was supported by a grant from the Asher Space Research Institute at the Technion.

REFERENCES

- Abraham, Z., Falceta-Goncalves, D., Dominici, T. P., Nyman, L.-A, Durouchoux, P., McAuliffe, F., Caproni, A., & Jatenco-Pereira, V. 2005, *A&A*, 437, 977
- Akashi, M., Soker, N., & Behar, E. 2006, *ApJ*, 644., 451
- Andersen, A. C. 2007, Dust from AGB stars (astro-ph/0702618v1)

- Behar, E., Nordon, R., & Soker, N. 2007, *ApJ*, 666, L97.
- Corcoran, M. F. 2005, *AJ*, 129, 2018
- Corcoran, M. F., Ishibashi, K., Swank, J. H., & Petre, R., 2001, *ApJ*, 547, 1034
- Corcoran, M. F., Pittard, J. M., Stevens, I. R., Henley, D. B., & Pollock, A. M. T. 2004, in the Proceedings of "X-Ray and Radio Connections", Santa Fe, NM, 3-6 February, 2004 (astro-ph/0406294)
- Cox, P., Mezger, P. G., Sievers, A., Najarro, F., Bronfman, L., Kreysa, E., & Haslam, G. 1995, *A&A*, 297, 168
- Damineli, A. 1996, *ApJ*, 460, L49
- Damineli, A., Kaufer, A., Wolf, B., Stahl, O., Lopes, D. F., & de Araujo, F. X. 2000, *ApJ*, 528, L101
- Davidson, K., & Humphreys, R. M. 1997, *ARA&A*, 35, 1
- Duncan, R. A., & White, S. M. 2003, *MNRAS*, 338, 425
- Falceta-Goncalves, D., Jatenco-Pereira, V., & Abraham, Z. 2005, *MNRAS*, 357, 895
- Frank, J., King, A. R., & Raine, D. J. 1985, *Accretion Power in Astrophysics*, Cambridge Univ. press (Cambridge, UK).
- Gomez, H. L., Dunne, L., Eales, S. A., Edmunds, M. G., 2006, *MNRAS*, 372, 1133G
- Hamaguchi, K. Corcoran, M. F., Gull, T., Ishibashi, K., Pittard, J. M., Hillier, D. J., Damineli, A., Davidson, K., Nielsen, K. E., & Kober, Gladys Vieira 2007, *ApJ*, 663, 522
- Hildenbrand, R. H., 1983, *QJRAS*, 24, 267H
- Hillier, D. J., Davidson, K., Ishibashi, K., & Gull, T. 2001, *ApJ*, 553, 837
- Humphreys, R. M., Davidson, K., & Smith, N., 1999, *PASP* 111, 1124
- Ishibashi, K., Corcoran, M. F., Davidson, K., Swank, J. H., Petre, R., Drake, S. A., Damineli, A., & White, S. 1999, *ApJ*, 524, 983
- Kashi, A., & Soker, N. 2007a, *MNRAS*, 378, 16091618
- Kashi, A., & Soker, N. 2007b, *NewA*, 12, 590 (astro-ph/0702661v2)
- Krugel, E. 2003, *The Physics of Interstellar Dust*, Institute of Physics Publishing (Bristol and Philadelphia)
- Mitchell R.M., & Robinson G., 1978, *ApJ* 220, 841
- Lamers, H. J. G. L. M et al. 1996, *A&A*, 315, L229

- Nielsen, K. E., Corcoran, M. F., Gull T. R., Hillier, D. J., Hamaguchi, K., Ivarsson, S. & Lindler, D. J. 2007, (astro-ph/0701632)
- Pittard, J. M., & Corcoran, M. F 2002, A&A, 383, 636
- Rybicki, G. B., Lightmann, A. P. 2004, Radiative Processes in Astrophysics, Wiley-VCH
- Schaerer, D. & de Koter, A. 1997, A&A 322, 598
- Smith, N., 2005, MNRAS, 357, 1330
- Smith, N. 2006, ApJ, 644, 1151
- Smith, N. 2007, in Massive Stars: From Pop III and GRBs to the Milky Way ed. M. Livio (proceedings of STScI May Symposium 2006) (astro-ph/0607457)
- Smith, N., Davidson, K., Gull, T.R., Ishibashi, K., Hillier, D.J., 2003a, ApJ, 586, 432S
- Smith, N., & Ferland, G. J. 2007, ApJ, 655, 911
- Smith, N., Foley, R. J., & Filippenko A. V. 2007, arXiv:0704.2249
- Smith, N., & Gehrz, R. D., 1998, AJ, 116, 828, 1998
- Smith, N., Gehrz, R. D., Hinz, P. M., Hoffmann, W. F., Hora, J. L., Mamajek, E. E., & Meyer, M. R. 2003b, AJ, 125, 1458
- Smith, N, Owocki, S. P., 2006, ApJ, 645L, 45S
- Smith, N., Morse, J. A., Davidson, K., & Humphreys, R. M. 2000, ApJ 120: 920,934
- Smith, N., Morse, J. A., Collins, N. R., & Gull, T. R. 2004, ApJ, 610, L105
- Soker, N. 2003, ApJ, 597, 513
- Soker, N. 2005, ApJ, 635, 540
- Soker, N. 2007, ApJ, 661, 482
- Soker, N. & Behar, E. 2006, ApJ, 652, 1563
- Steiner, J. E., & Daminieli, A. 2004, ApJ, 612, L133
- van Genderen A. M., de Groot, M. J. H., & The R. S. 1994, A&A 283, 89
- van Genderen A. M. & Sterken, C. 2007, IBVS, 5782, 1
- van Genderen A. M., Sterken, C., Allen, W. H., & Walker, W. S. G. 2006, JAD, 12, 3
- Verner, E., Bruhweiler, F. & Gull, T. 2005, ApJ, 624, 973
- Walsh, A.R., & Ageorges, N., 2000, A&A 357, 255
- Whitelock, P. A., Feast, M. W., Marang, F., & Breedt, E. 2004, MNRAS, 352, 447

Whittet, D.C.B., 2003, *Dust in the Galactic Environment Second Edition*, Institute of Physics Publishing (Bristol and Philadelphia)

Woitke, P., Kruger D., Sedlmayr, E 1996, *A&A*, 311, 927

Zanella, R., Wolf, B., & Stahl, O. 1984, *A&A*, 137, 79

A. Appendix: Free-Free Absorption Calculations:

We now show that the dense post-shock primary wind material (the conical shell) cannot absorb enough of the J -band emission (for more detail on the absorption by the conical shell see Kashi & Soker 2007a). The free-free absorption coefficient at frequency ν is given by equation (5.18) of Rybicki & Lightmann (2004)

$$\alpha_{\nu}^{ff} = 3.7 \times 10^8 T^{-\frac{1}{2}} Z^2 n_e n_i \nu^{-3} \left[1 - \exp\left(-\frac{h\nu}{KT}\right) \right] g_{ff} \text{ cm}^{-1}, \quad (\text{A1})$$

where, as discussed in the section 2.2, $T = 10^4$ K and $g_{ff} \simeq 1.2$. We calculate the free-free optical depth for the J -band as a function of α (the angle between a direction opposite to the direction of the primary to a point on the contact discontinuity measured from the secondary; see Fig. 10 below) and θ (the orbital angle; see Fig. 9 below). Defining d as the post shock primary wind depth (see Kashi & Soker 2007a, and Fig. 10 below) we find that

$$\tau_{\nu}^{ff} = 2.2 \times 10^{-37} n_e(\alpha, \theta) n_i(\alpha, \theta) d(\alpha, \theta), \quad (\text{A2})$$

where n_e , n_i and d are in c.g.s. units. Figure 8 shows The free-free optical depth in the J waveband as a function of α and θ . The maximum value of τ_{ν}^{ff} is obtained for a direction through the primary ($\alpha = 180^\circ$) at periastron ($\theta = 0^\circ$). For the point on the conical shell along this direction the electron and ion densities are $n_e \sim 1.9 \times 10^{12} \text{ cm}^{-3}$, and $n_i \sim 1.6 \times 10^{12} \text{ cm}^{-3}$, respectively, and the geometrical width of the conical shell along this direction is $d \sim 2.5 \times 10^{11} \text{ cm}$. The maximum value obtained is therefore $\tau_{\nu}^{ff} \sim 0.17$. We note that this is an hypothetical maximum, because according to our model the colliding winds cone does not exist close to periastron passage. We conclude that the dense post-shock primary wind (the conical shell) is optically too thin to absorb enough of the J -band emission as seen in observations.

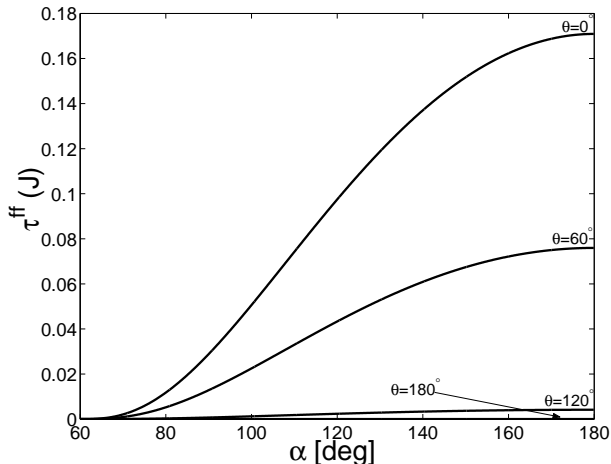


Fig. 8.— The free-free optical depth in the J waveband as a function of α and θ as given by equation A2. α is the angle of a ray through the conical shell measured from the secondary ($\alpha = 180^\circ$ toward the primary; see Fig. 10 below), and θ is the orbital angle ($\theta = 180^\circ$ at apastron and $\theta = 0^\circ$ at periastron).

B. Appendix: Ionization and Dust Formation in the Colliding Winds Cone:

In finding the ionization front location we use our colliding winds model (Kashi & Soker 2007a) and assume that dust forms in the post-shock primary wind region. We define the direction angle α as the angle from a direction opposite to the primary direction to a point on the contact discontinuity as measured from the secondary (see Fig. 10). Segments of the conical shell start to be neutral when the total recombination rate per steradian along a direction α measured from the secondary becomes equal or larger than the rate of ionizing photons ($h\nu \geq 13.6\text{eV}$) emitted by the secondary star per steradian, \dot{N}_{i2} . For the secondary of η Car $\dot{N}_{i2} = \dot{\Phi}_2/4\pi = 2 \times 10^{48}\text{s}^{-1}\text{sr}^{-1}$, as derived by Kashi & Soker (2007a) based on Schaerer & de Koter (1997). We neglect recombination in the low density secondary wind. Thus the distance along the line from the contact discontinuity through the shocked primary wind where the wind is optically thin to the secondary’s radiation, as can be seen in Fig. 11, is

$$d_{\text{abs}} = \frac{\dot{N}_{i2}}{\alpha_B n_e n_H r_2^2} \tag{B1}$$

where α_B is the recombination coefficient, r_2 is the distance to the secondary, n_e is the electron number density and n_H is the proton number density.

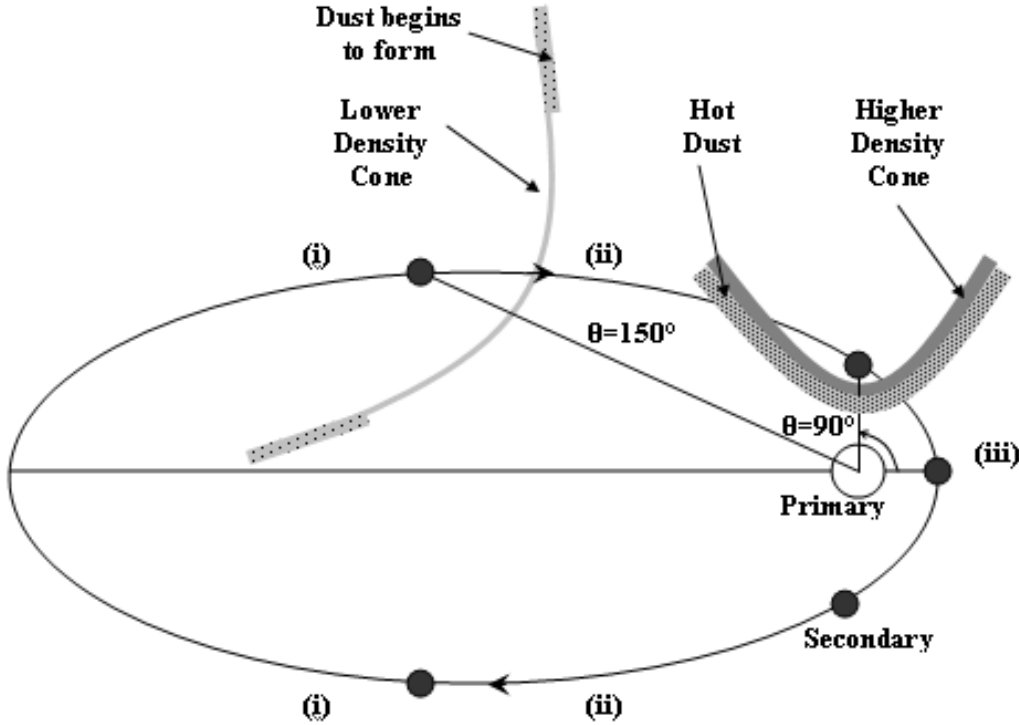


Fig. 9.— The three stages of the conical shell ionization plotted along the secondary’s orbit together with the orbital phases of transitions between stages. Darker colors means denser wind. Stage *(i)*: When the orbital separation is large, the hot secondary ionizing radiation manages to keep the conical shell (the post-shock primary wind zone) totally ionized. In that stage dust can be formed only at very large distances. Stage *(ii)*: When the orbital separation decreases to $r \lesssim 14.3$ AU at ~ 170 days ($\theta = 150^\circ$) before (after) periastron, the density of the gas in the conical shell increases, the cone becomes optically thick to the secondary’s UV radiation and parts of the cone begin to be neutral. First at large distances, and then closer and closer to the stagnation point along the line joining the two stars. Stage *(iii)*: As the secondary approaches periastron, $r \lesssim 3.2$ AU at ~ 20 days ($\theta = 90^\circ$) before (after) periastron the ionization front is within the conical shell in all directions, and the region near the stagnation point becomes neutral. During most of this stage the conical shell does not exist according to our model. Instead, an accretion flow onto the secondary takes over. The exact times (and locations) of the transitions between the stages depend on poorly determined winds’ parameters.

We recall that the ionizing radiation from the primary is neglected here because most of it is absorbed in the dense gas of the primary wind close to the primary, and in the dense

gas in the conical shock region. Despite being five times as luminous as the secondary, the primary is much cooler and its ionizing photon flux ($h\nu > 13.6$ eV) is small to begin with. However, at longer wavelengths in the UV and in the visible band the primary radiation cannot be neglected, and it is considered as a heating source of the dust together with the secondary radiation (see discussion following equation 7).

The value of $d_{\text{abs}}(\alpha)$ is then compared to the thickness $d(\alpha)$ of the wind in the same direction α . In stage (i) $d_{\text{abs}} > d$ for every α and the shocked primary wind (the conical shell) is totally ionized. In stage (ii) $d_{\text{abs}} > d$ for small values of α and $d_{\text{abs}} < d$ for large values of α , and parts of the cone begin to be neutral. In stage (iii) $d_{\text{abs}} < d$ for every α and the ionization front is within the conical shell in all directions. These three stages are drawn schematically in Figs. 9 and 10.

When the material in the conical shell is neutral, the conditions are favorable for dust to be formed. The gas in the conical shell is initially hot $T_{\text{gas}} = 10^4$ K. As it expands and cools, hot dust forms at temperatures $T \lesssim 1700$ K (Van Genderen et al. 1994). The cooling time depends on density. We use figure 11 of Woitke et al. (1996) to estimate the cooling time from $T = 10^4$ K and $n \simeq 10^{12} - 10^{14}$ cm $^{-3}$ to $T = 1700$ K in an adiabatic process and find it to be approximately 5 – 10 days.

For most of the orbital period the wind is ionized and no dust is being formed in the conical shell close to the secondary. The roughly constant IR emission is emitted by dust which was formed in previous cycles, mostly cooler dust, and the hotter dust that is formed in the primary wind and heated by the secondary and primary radiation. The rapid increase in the IR emission ~ 150 days before the 2003.5 event (see section 7) can be explained by the process described in stage (ii) - more and more material in the conical shell becomes neutral, favoring the formation of dust closer to the secondary. The occurrences of the event are explained in section 7.

We stress again that the numbers can be somewhat different for other parameters, like e , stellar masses and magnetic field in the primary wind.

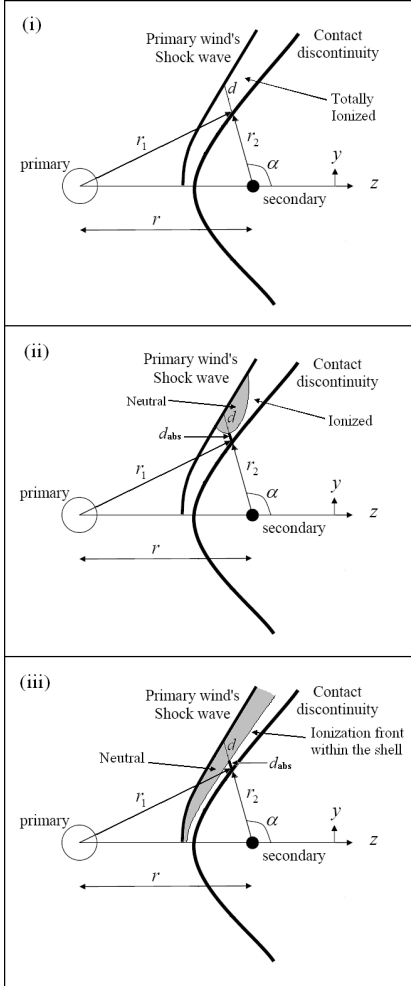


Fig. 10.— Schematic drawing of the plane between the two stars, at the three stages of the conical shell ionization. d is the thickness of the shocked primary wind zone (conical shell) from the contact discontinuity to the primary shockwave in α direction. d_{abs} is the distance along the line from the contact discontinuity through the shocked primary wind where the wind is optically thin to the secondary’s radiation, in the same direction. Upper panel – Stage(i): Until ~ 170 days before (after) periastron $d_{\text{abs}} > d$ for all values of α . The secondary ionizing radiation manages to keep the conical shell totally ionized. Middle panel – Stage(ii): From ~ 170 days until ~ 20 days before (after) periastron $d_{\text{abs}} > d$ for small values of α and $d_{\text{abs}} < d$ for large values of α , and parts of the cone begin to be neutral. Lower panel – Stage(iii): From ~ 20 days before periastron until ~ 20 days after periastron $d_{\text{abs}} < d$ for every α and the ionization front is within the conical shell in all directions, and the region near the stagnation point becomes neutral. The last stage exists only for a short period of time, or might not exist at all, because of the collapse of the conical shell onto the secondary ~ 20 days before periastron, and the formation of an accretion flow (Akashi et al. 2006).

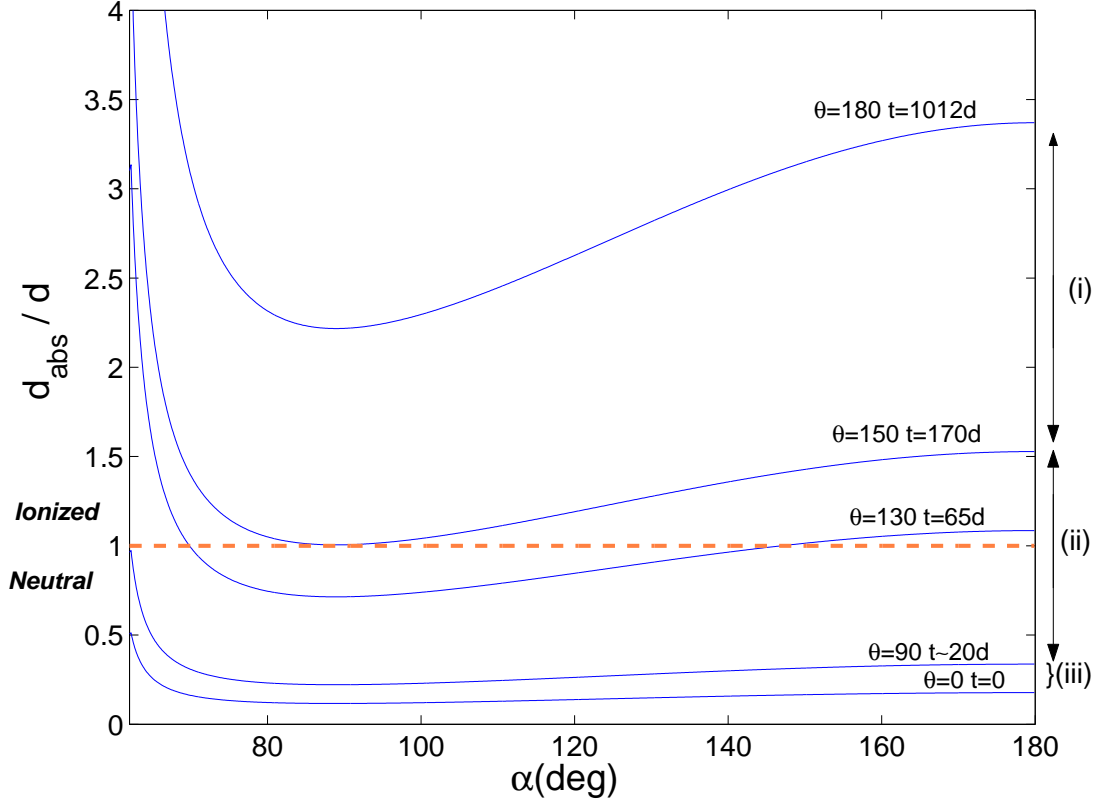


Fig. 11.— $d_{\text{abs}}(\alpha)$ is the distance along the line at angle α from the contact discontinuity through the shocked primary wind (conical shell) required to absorb the ionizing radiation of the secondary star. In our model the asymptotic angle of the conical shell is at $\alpha = 60^\circ$ (left side of the figure), where $\alpha = 180^\circ$ is the angle toward the primary and $\alpha = 0^\circ$ in a direction opposite to the primary. $d(\alpha)$ is the total length through the conical shell along the same direction (see Fig. 10). If $d_{\text{abs}}(\alpha)/d(\alpha) > 1$ then the conical shell along the direction α is completely ionized, while if $d_{\text{abs}}(\alpha)/d(\alpha) < 1$ part of the conical shell is neutral. Neutral regions are more favorable for dust formation. θ is the orbital angle (see Fig. 9), with $\theta = 0$ at periastron ($t = 0$), and $\theta = 180^\circ$ at apastron ($t = 1012$ days). The three stages discussed in the text, and the times (in days) before periastron passage of transitions between the stages are marked on the figure.